

Three- dimensional Effects in Electrical Impedance Tomography

M. Wang

Department of Electrical Engineering and Electronics*
UMIST. P.O. Box 88, Manchester M60 1QD, UK

M. Wang is the member of the Virtual Centre for Industrial Process Tomography

Abstract – An investigation of 3-dimensional (3D) effects on electrical impedance tomography is reported. 3D effects in measurement, simulation and analytical models are described. A 3D attenuation range (75% attenuation) from the sensing plane is suggested as one third of process vessel's diameter. The imaging trajectory of an axially moving object is found towards the central axis of a process vessel when a 16-electrode sensing ring is employed. The paper also reports the use of a guarded electrode scheme can reduce the imaging displacement but has no evident effects at the compressing the sensing space.

Keywords : 3D sensing space, Attenuation ratio, 3D-convergence effect, Single-plane sensor, Guarded electrode scheme.

1. INTRODUCTION

Electrical resistance tomography has been employed as a visualization tool for mixing processes, multi-phase flow and aqueous-based separation in chemical engineering. Single sensing ring strategies and two-dimensional (2D) electric field reconstruction algorithms are adopted in the most applications. However, the reconstructed images are affected by the three dimensional (3D) distribution of the actual field in the sensing domain if the dimension of sensing electrodes along the pipeline is restricted. A guarded electrode scheme has been reported to reduce the 3D effects [1]. However, some researchers concluded that a guarded system has no advantages over an unguarded system [2]. A number of other approaches have also been developed to reduce the 3D effects, such as a multi-plane sensing strategy [3] and a full 3-D approach [4]. This paper focuses on the 3D effects from a 2D electrical tomographic measurement scheme.

Results from measurement, simulation and analysis are reported for evaluation and comparison of the 3D effects inhered with the single-plane sensing scheme and the guarded-electrode sensing scheme.

2. MEASUREMENT

To compare the 3D effects from a typical 16-electrode sensing configuration and the sensor with guarded electrodes configuration, a Perspex vessel mounted with four planes of 16-electrodes is employed in Figure 1. For collecting data with regard to a typical single-plane sensing configuration, only the bottom sensing ring, as shown in Figure 1, is connected and the other are suspended without any connection. For observing the effect of the guarded electrode scheme, the electrodes in the top three rings are simultaneously driven by voltage buffers with voltage-drops at the related source/measurement electrodes in the bottom sensing plane. The conductivity of electrolyte in all experiments is 0.1ms/cm. Two nonconductive plastic golf balls ($f=4\text{cm}$) are used as the imaging targets in these experiments. A 3mA current @ 9.6 kHz frequency is used in all measurements.

To investigate the attenuation along the centre axis line (A) and the halfway line (B) in Figure 1, data are acquired in 9 steps as the ball is moved from the sensing plane to the top of the vessel. Measurements are obtained from the setups using both the single-plane sensor and the guarded electrode scheme.

• M. Wang' present address: School of Process, Environmental and Material Engineering, University of Leeds, Leeds LS2 9JT, Tel: 0113 243 1751.

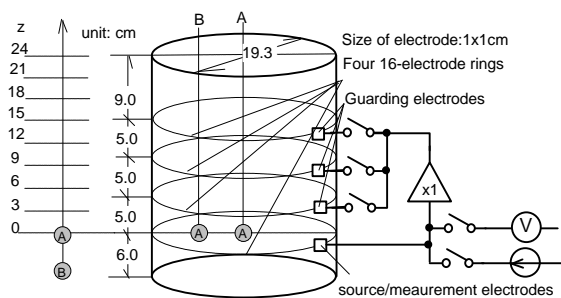


Figure 1: Sensor configuration and measurement setup

Figure 2 shows the attenuation of the maximum relative changes of voltage measurement. Before the ball reaches 6cm from the bottom plane, the attenuation from the single-plane sensor, without guarding electrodes, drops more quickly than for the guarded electrode scheme. Particularly, a high speed attenuation occurs when the ball is moved along the halfway B. Due to the effect of the guarding electrode scheme, the attenuation from the guarded electrode scheme has a linear relationship before the ball comes within 6cm from the bottom sensing plane.

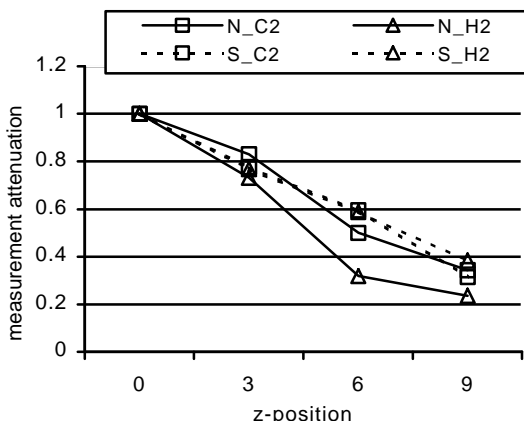


Figure 2: Voltage measurement attenuation due to a movement of a ball from the bottom sensing plane (as a reference) to the fourth sensing plane of the vessel. (N_C2 and N_H2: obtained using the non-guarded sensor along the central axis A and the halfway B, S_C2 and S_H2: obtained using the guarded sensor along the central axis A and the halfway B).

The ball's position has been reconstructed and reflected in a conductivity change using the sensitivity theorem method (STM) [5] from these data. The conductivity attenuation data from the ball at the bottom sensing plan are given in Figure 3. The attenuation speed is similar as that obtained from measurements (Figure 2) and a much slower change of the attenuation from the guarded

electrode scheme is observed below 3cm. This is evidently caused by the effect of driven electrodes in the scheme. The reconstructed conductivities drop into a noise zone between 0.095 to 0.105mS/cm for distances larger than 6cm because only a limited signal-to-noise ratio (SNR), about 2.4%, can be achieved from the guarded electrode scheme and then adapted to the single-plane sensing strategy for the consistency in comparison of the results. The reason for the low SNR presented in the data from the guarded electrode scheme is because the guarded (driven) electrodes introduce an inconsistency to the original field, which is mainly caused from the stray capacitances of the voltage buffers and their related circuits used in the scheme.

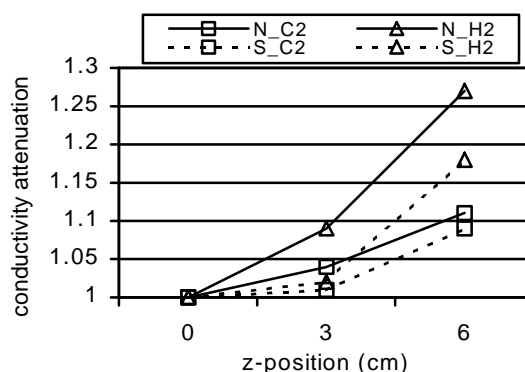


Figure 3: Attenuation of the relative change of reconstructed conductivity due to a movement of a ball from the bottom sensing plane (as a reference) to the fourth sensing plane of the vessel. (N_C2 and N_H2: obtained using the non-guarded sensor along the central axis A and the halfway B, S_C2 and S_H2: obtained using the guarded sensor along the central axis A and the halfway B).

To reveal the 3D effect on imaging the ball's trajectories, the sequences of the 2D conductivity maps are interpolated to the 3D images as shown in Figure 4. In order to view the maximum low conductivity (ball profile) at horizontal cross sections, a grayscale-banded process is applied to these images. The trajectory can be easily drawn out at the vertical cross section based on these maximum changes. It is found that the trajectory of the ball has been distorted towards the center of the vessel's axis when the single-plane sensor is applied (Figure 4b), that is recognized as the *3D-convergence effect*. The trajectory with less distortion is presented from the data obtained from the guarded electrode scheme (Figure 4d). However, all images obtained from the guarded sensor have enlarged ranges along the z-direction, which has already been explored in the first part of the section due to the slow attenuation.

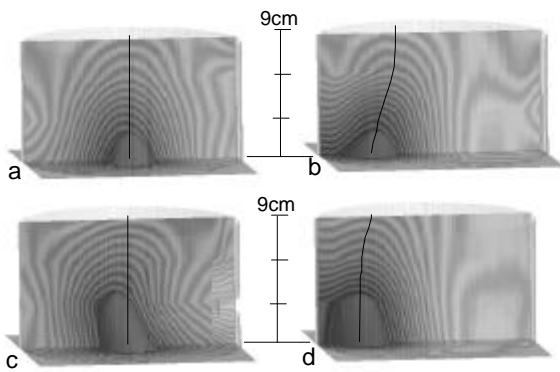


Figure 4: 3D attenuation speed and convergence effects presented from imaging a moving ball ((a)(b): using a single-plane sensor, (c)(d): using guarded electrode scheme, (a)(c): along the central axis A, (b)(d): along a halfway B). The dotted lines denote the ball's trajectories. The grayscale-banded lines denote the maximum low conductivity at the horizontal cross sections.

The 3D attenuation speed and convergence effect could be reflected more clearly if the data has a low SNR. Figure 5 shows a sequence of slice images obtained from the ball's movement along the halfway B of the vessel. The SNR presented in these data is 0.4%. Figure 5a and 5b show the images reconstructed using the sensitivity back-projection method [5] and presented using individual grayscale scales [5] and a common grayscale (b). The 3D-convergence effect can be easily observed from Figure 5a and the attenuation is straightforward reflected in Figure 5b, both of which are plotted in Figure 5c and 5d respectively.

Based on the measurements obtained from the experiment setups using the single-plane sensor, the effected 3D range (75% attenuation) from the sensing plane is about one third of the vessel diameter. An image displacement in terms of convergence effect is approximately linear in the attenuation range.

Images with less displacement are present from the data obtained using the guarded electrode scheme. However, the low speed of attenuation from the guarded electrode scheme would produce results with a poor 3D distinguishability. The driven electrodes also produce a complex field distortion, which result in a poor SNR in these measurements.

The attenuation given from the single-plane sensor is faster than those from the guarded electrode scheme, which may imply its better 3D

distinguishability compared with the guarded electrode scheme.

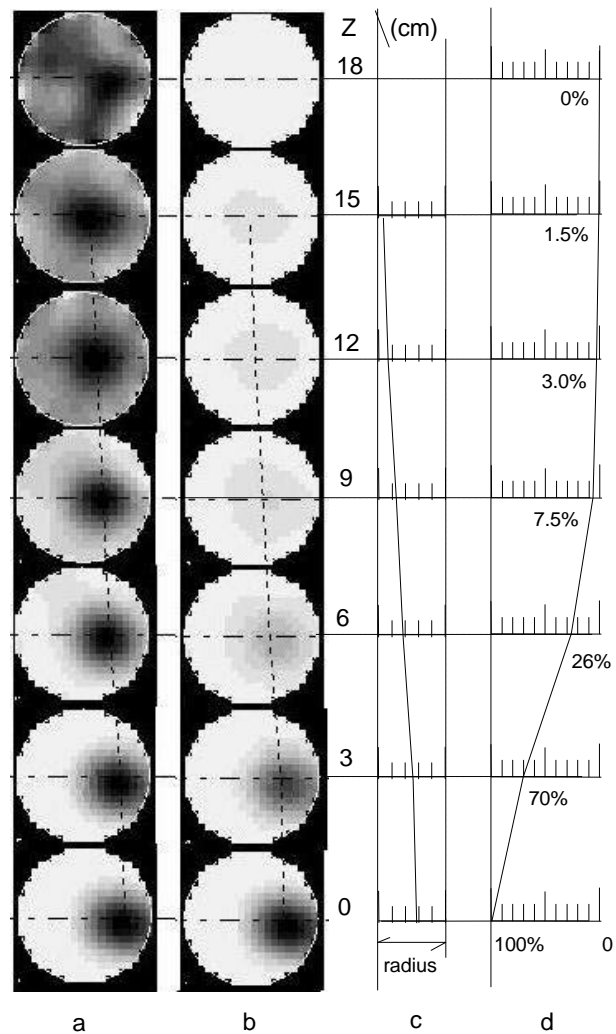


Figure 5: 3D attenuation speed and convergence effects presented from imaging a moving ball with low SNR data at 0.4% (a: using individual grayscale, b: using a common grayscale, c: 3D convergence effect, d: 3D attenuation).

3. SIMULATION

A series of simulations have been performed using Ansoft Maxwell 3D-Electrostatic simulation package. To simplify the simulation models, it is assumed that the potentials at guarding electrodes in a static condition have same values as those at the related source electrodes (refer to Figure 1). Two of simulated electrode configurations and process vessels are shown in Figure 6, which are related to a single-plane sensor (Figure 6a) and a long driven source electrode scheme (Figure 6b), respectively. The dimension of vessel in the

simulation is the 30cm of the height and the 15cm of the diameter. The conductivity of the “vessel” is 0.1mS/cm. A current source applied to one pair of the electrodes and the differential voltages are measured from another pair of electrodes when a conductive cube (2×2×2cm) is moved in 4 steps along a halfway B from the sensing plane to the top of the vessel.

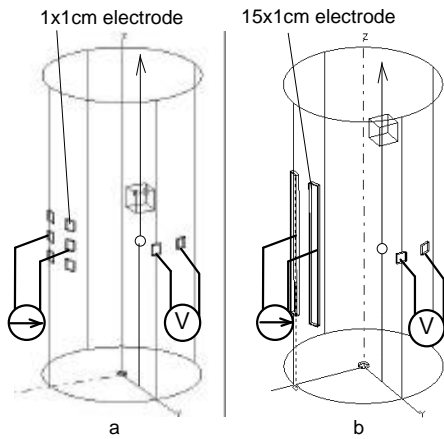


Figure 6: Configurations in simulation

Results are shown in Figure 7. The attenuation speed before 5cm from the single-plane sensor is little faster than that from the guarded electrode scheme.

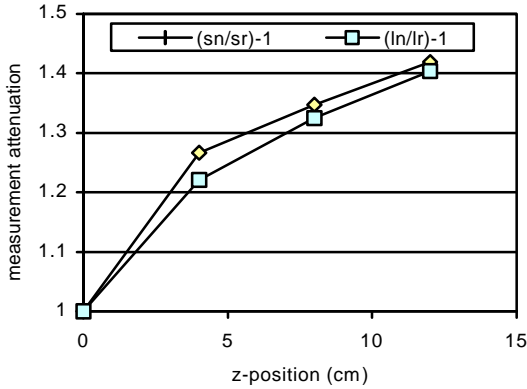


Figure 7: Attenuation of voltage measurements simulated from a moving cube along a halfway between the axis and the edge of the vessel (sn/sr-1: field excited from the short electrode, ln/lr-1: filed excited from long electrode pair). The error energy is 1% from the simulation.

4. ANALYSIS

It is known that the tomographic sensitivity of a four terminal system is proportional to the scalar multiplication of two electric field intensity vectors,

which are generated from two current sources [6]. The expressions of the relationship are given in Eq.1 and Eq.2 in term of the sensitivity coefficient [6] and the sensitivity density [7] respectively. To simplify the analytical problem, an electrostatic model with two point-charge pairs orthogonal to the X-axis at the XOY plane are employed (Figure 8). Assuming the length of the point-charge pairs, l , to be far smaller than the distances of r_1 and r_2 ($l \ll r_1$ and $l \ll r_2$), the field vector produced by a charge pair at the position $P(x,0,z)$ can be described by Eq.3 [8] where the vector along z -direction is zero at the XOZ plane.

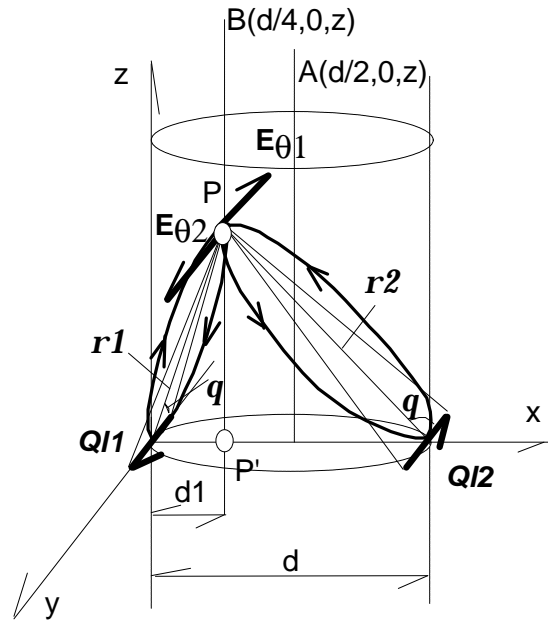


Figure 8: Electrostatic model

$$S_{fy} = - \int_{a_p} \frac{\nabla f}{I_f} \cdot \frac{\nabla y}{I_f} da_p \quad (1)$$

$$D_{fy,p} = -\nabla f \cdot \nabla y = -E_{f,p} \cdot E_{y,p} \quad (2)$$

$$E = a_r \frac{Ql \cos q}{2\pi \epsilon r^3} + a_q \frac{Ql \sin q}{4\pi \epsilon r^3} \quad (3)$$

Since the angle θ is $\pi/2$ for position P at the XOZ plane, only a_θ component exists (Eq.4). Therefore, the sensitivity density of two charge pairs at the position P is derived as Eq.5.

$$E = a_q \frac{Ql}{4\pi \epsilon r^3} \quad (4)$$

$$D_{Ql1,Ql2,P} = -\mathbf{E}_{Ql1,P} \cdot \mathbf{E}_{Ql2,P} = \left(\frac{Ql}{4\pi\epsilon} \right)^2 \frac{1}{\mathbf{r}_1^3 \cdot \mathbf{r}_2^3} \quad (5)$$

From the superposition principle, the ratio between the two electric intensity fields at the position P(d1,0,z) implies the *convergence ratio*, \mathbf{h} , at the position P'(d1,0,0) reconstructed from a 2D algorithm (Eq.6). The convergence ratio, as given in Eq.6, should be one if the reconstructed position P' has the same distance to the two point-charge pairs ($\mathbf{r}_1 = \mathbf{r}_2$). The convergent ratio can be derived to be 1 if $z \rightarrow \infty$ in Eq.6, which means the reconstructed position P', if the field intensity could be detectable, will be move towards the centre of the distance d if $z \rightarrow \infty$.

The *attenuation ratio*, \mathbf{x} , between the sensitivity densities at positions P(d1,0,z) and P'(d1,0,0) is used to describe the sensitivity attenuation along the z-direction (Eq.7).

$$\mathbf{h} = \frac{|E_{q2}|}{|E_{q1}|} = \left(\frac{\mathbf{r}_1}{\mathbf{r}_2} \right)^3 = \left[\frac{z^2 + d_1^2}{z^2 + (d - d_1)^2} \right]^{\frac{3}{2}} \quad (6)$$

$$\mathbf{x} = \frac{D_P}{D_0} = \left(\frac{d_1 \cdot (d - d_1)}{\mathbf{r}_1 \cdot \mathbf{r}_2} \right)^3 = \left[\frac{d_1^2 \cdot (d - d_1)^2}{(z^2 + d_1^2) \cdot [z^2 + (d - d_1)^2]} \right]^{\frac{3}{2}} \quad (7)$$

The values of \mathbf{h}_1 and \mathbf{x}_1 ($d_1=d/2$) along a central line A and \mathbf{h}_2 and \mathbf{x}_2 ($d_1=d/4$) along an off-centre line B are plotted in Figure 9. The convergence ratios are always one along the central line and towards one along the off-center line if $z \rightarrow \infty$. The sensitivity attenuation along the off-center line is faster than that along the central line.

With regard to the guarded electrode scheme in a static condition, a linear charge pair along the Y-axis is employed to replace the point-charge pair in Figure 8. Since the intensity of the electric field generated from a linear charge pair only related to variables along x- and y-directions, the convergence ratio and attenuation ratio along the z-direction have been governed by the point-charge pair Q/2. The attenuation ratios given from this configuration are much slower than those from the two point-charge pairs. Instead of the convergent effect in two point-charge pairs configuration, the imaging trajectory has been affected with lower divergence, which will not be discussed further in this paper.

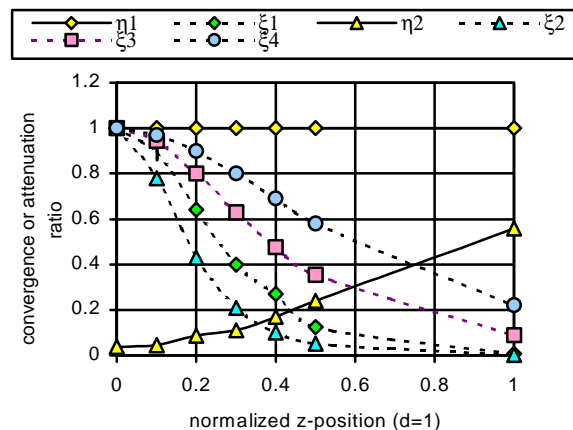


Figure 9: Convergence ratio and attenuation ratio derived in the analytical model (generated from point-charge pairs: η_1, ξ_1 along the line A and η_2, ξ_2 along the line B; generated from a linear charge pair and a point-charge pair: ξ_3 along the line A and ξ_4 along the line B)

In the case of the electric field generated from two linear-charge pairs, the results will not be affected by the 3D effects because the field distribution can be described as a full 2D electric field without 3D distinguishability.

5. DISCUSSION

Results from the investigation show the tomographic measurements to be highly affected from the 3D field distribution, which mainly consist of the 3D field attenuation and image convergence effects. Nevertheless, due to a fast attenuation in the range of one third of the vessel's diameter, the image distortion would not give a fatal problem for a fixed volume measurement (e.g. mixing processing) using a multi-plane sensing strategy [3] or a flow measurement employing fast data collection.

To demonstrate the 3D effects on flow measurement, a sequence of tomographic images are measured from the movement of two Golf balls (A and B in Figure 1) from the bottom to the top of the vessel with the configuration of a single-plane sensor. The images are reconstructed using the sensitivity back-projection method [5] and interpolated using the SpyGlass image-processing package. The distinguishable distance, as shown in Figure 10, between the nearest surfaces of the two balls is 5cm (side-side), which is about 25% of the vessel diameter. The result is achieved with data had 1% SNR. The convergence effect can still be observed from the position of the blurring

shadow between the two balls' images. Its trajectory is drawn in dotted line.

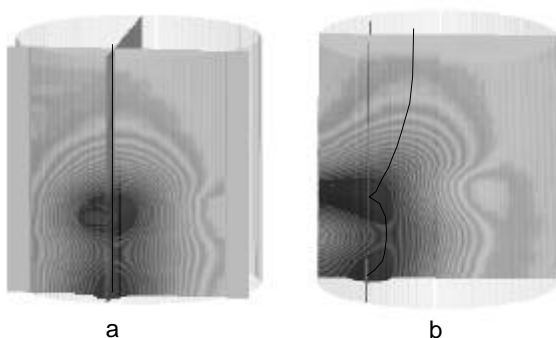


Figure 5: Imaging two Golf balls' movement

The attenuation of the sensitivity density generated from the single-plane sensor is faster than that from the guarded electrode scheme in the experiment, which implies that the conventional single-plane sensor will provide a better distinguishability along z-direction than that from the guarded electrode scheme. However, there is a smaller convergence effect in the case of use of the guarded electrode scheme, but the SNR could be reduced by the multi-source effects.

Synthesizing the results from measurements, simulation and analysis, the guarded electrode scheme appears no evident effects at compressing the sensing space without a high cost at SNR, although an 'ideal guarding' as suggested [1] has not been fully constructed in the experiment, neither the distance between the measurement electrodes and the guarding electrodes nor the current constraint at the guarding electrodes.

6. CONCLUSIONS

3D distribution of electric field can produce significant effects to 2D tomographic imaging scheme: the limited 3D distinguishability and distorted imaging position. The attenuation range (75% attenuation) from the sensing plane is about one third of the diameter of the process vessel from the sensing plane. A convergence effect is also applied to images obtained from the 2D tomographic scheme. Due to a fast attenuation in the near range of the sensing plane, a multi-plane sensing strategy or fast measurement protocol can reduce the error caused by the 3D effect in electrical impedance tomography. The use of a guarded electrode technique can reduce the imaging displacement error but has no evident effects at compressing the sensing space.

REFERENCES

- [1] Ma, Y., Wang, H., Xu, L. and Jiang, C., "Simulation study of the electrode array used in an ERT system", Chem. Eng. Sci. Vol. 52, No. 13, 1997, pp.2197-2203.
- [2] Webster, J.G., "Electrical Impedance Tomography", Adam Hilger, Bristol, 1990.
- [3] Holden, P.J., Wang, M., Mann, R., Dickin, F.J. and Edwards, R.B., "Imaging stirred-vessel macromixing using electrical resistance tomography", AIChE, Apr. 1998, pp. 780-790.
- [4] Pinheiro, P.A.T., Loh, W.W. and Dickin, F.J., "Three-dimensional reconstruction algorithm for electrical resistance tomography", IEE proc.-Sci. Meas. Technol. **145** (3), 1998, pp85-93.
- [5] Wang, M., Mann, R. and Dickin, F., "Electrical resistance tomographic sensing systems for industrial applications", Chem. Eng. Comm., in press, May 1998, pp. 1-22.
- [6] Geselowitz, D.B., "An application of electrocardiographic lead theory to impedance plethysmography", IEEE Trans. Biomed. Eng., Vol. BME-18, Jan. 1971, pp 38-41.
- [7] Wang, M., Dickin, F.J., and Williams, R.A.: "Modelling and analysis of electrically conducting vessels and pipelines in electrical resistance process tomography", IEE Proc. Sci. Meas. Technol., **142** (4), July 1995 pp. 313-322
- [8] Kraus, J.D., "Solution of electromagnetics", Book Company Inc., 1990.